Topological Friction: Insight from Dynamics of a Test Chain in a Fixed-Topology Polymer Network

Zhenhua Wang,[1] Yuyuan Lu,[2,1,*] Lijia An,[1] and Zhen-Gang Wang[3]
[1]State Key Laboratory of Polymer Science and Technology, Changchun Institute of Applied Chemistry, Chinese Academy of Sciences, Changchun 130022, People's Republic of China
[2]Institute of Polymer Science and Engineering, Department of Chemical Engineering, Tsinghua University, Beijing 100084, People's Republic of China
[3]Division of Chemistry and Chemical Engineering, California Institute of Technology, Pasadena, California 91125, United States

(Received 20 February 2026; revised 15 May 2026; accepted 21 May 2026; published 16 June 2026)

The tube model has long served as a cornerstone of entangled polymer dynamics and rheology. We test some of the key concepts of the tube model by investigating the equilibrium dynamics of a free chain in a fixed-topology polymer network using molecular dynamics simulation. Our results reveal significant position-dependent dynamical heterogeneity manifested as a rugged free energy landscape for the longitudinal motion, resulting in additional friction due to the topological interactions, and a "tube dilation" mechanism arising from the relaxation of entanglements formed by loop strands in the network in a "flip-flop" motion. On timescales less than the Rouse time, the mean-square displacement of the center of mass of the free chain displays a subdiffusive behavior that is slower than the expected $t^{1/2}$ scaling. On longer timescales, the effects of topological friction amount to a renormalized monomer friction that is several times the intrinsic value. These results challenge some of the fundamental assumptions of the tube model, even under equilibrium conditions.

DOI: 10.1103/cpp1-j6lc

The motion of polymer chains in topologically restrictive environments is a fundamental challenge in polymer physics and rheology [1–4]. Edwards [5,6] first introduced the concept of the "tube" to explain chain dynamics in cross-linked polymers. Building upon this, de Gennes [7] described the motion of a free chain in a fixed gel network and proposed the concept of reptation, suggesting that a similar tube structure exists in uncross-linked polymer melts. In this framework, a polymer chain is envisioned to follow Rouse dynamics along a coarse-grained contour known as the primitive path (PP) defined by the network. Among other things, this model leads to distinct behaviors in the mean-square displacement of a single monomer, $g_1(t)$, and the center of mass of a tagged chain, $g_3(t)$, across different timescales for $\tau_e < t < \tau_R$, $g_1(t) \propto t^{1/4}$, and $g_3(t) \propto t^{1/2}$, where τ_e and τ_R are the Rouse times for an entanglement strand and the entire chain, respectively.

Doi and Edwards [1] further advanced the tube model by providing a mathematical framework that simplifies the complex topological interactions in entangled polymer melts. They proposed that, as in a fixed network, a test chain experiences Rouse dynamics within the tube, moving along the PP while being restricted in its lateral motions. This picture has become the molecular foundation for polymer dynamics and rheology in entangled polymer systems [8,9]. However, rigorous molecular-level validation of this model remains lacking, due to the complexities inherent in the multichain nature of topological interactions. For example, the assumption of uniform friction for local and curvilinear Rouse motion within the tube has yet to be tested [10]. Moreover, as highlighted in the seminal Doi-Edwards treatise [1], a longstanding discrepancy persists: tube sizes inferred from direct rheological measurements are considerably larger than those extracted via neutron or x-ray scattering. This mismatch points to unaccounted-for time dependence in entanglement constraints, underscoring the critical need for a more comprehensive framework to describe tube size determinants and the interplay between longitudinal and transverse topological constraints.

The molecular mechanisms underlying these unresolved issues have received significant attention [11–15]. Schweizer *et al.* [16,17] developed a dynamical mean-field theory that yields a molecular expression for the transverse tube potential for entangled polymers; their work predicts that the confinement potential for the PP is highly anharmonic. Complementary molecular dynamics simulations by Zhou and Larson further showed that initial tube confinement softens over time due to chain-end-mediated constraint release [18]. Beyond refinements to existing frameworks, some researchers have challenged the core

*Contact author: yylu@ciac.ac.cn

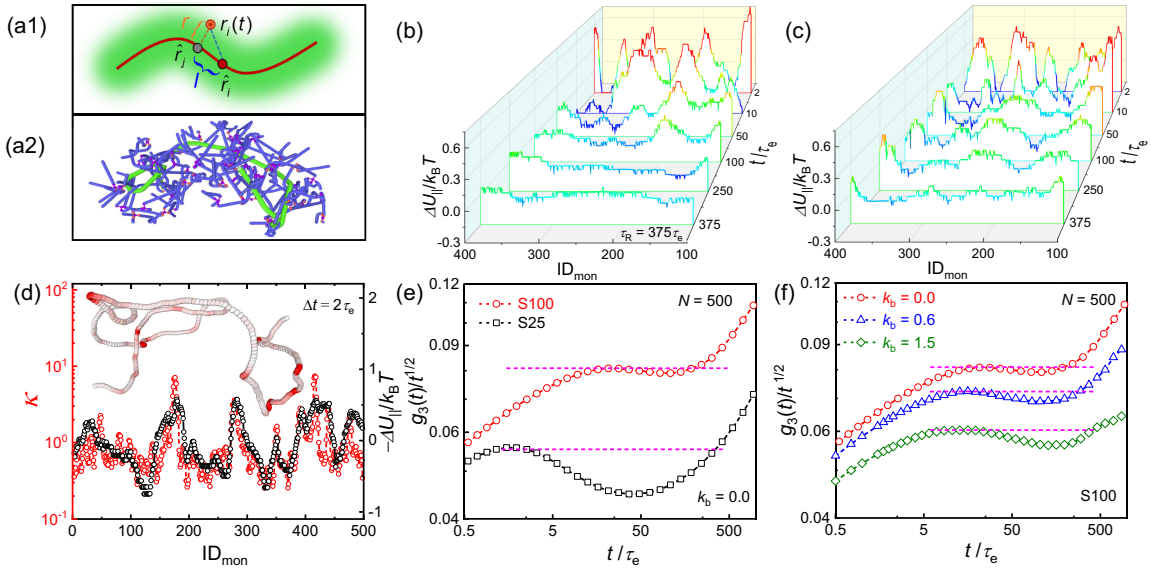

FIG. 1. Longitudinal constraints. (a1) Molecular cloud generated from isoconfigurational conformations around the PP of the test chain. (a2) Snapshot of the test chain in a cross-linked network. (b), (c) Longitudinal potential $\Delta U_{\parallel}$ as a function of monomer rank $\mathrm{ID}_{\mathrm{mon}}$ for two test chains at different timescales. (d) Correlation between the potential and local curvature of the PP chain, κ. (e) Mean-square displacement of the center of mass of the test flexible chain, $g_3(t)$, in networks of different strand lengths ($S = 25$ and 100, denoted as S25 and S100). (f) Comparison of $g_3(t)$ for test chains with varying stiffness ($k_b = 0.0$, 0.6, and 1.5).

assumptions of reptation and tube models, arguing that entangled dynamics are dominated by cooperative many-chain interactions [14,15] rather than single-chain topological constraints. Additionally, there have been ongoing debates regarding several nonlinear rheological phenomena [19–21]. For example, the retarded relaxation of entangled polymers following large step deformation [22–24] raises questions about whether polymer chains follow free Rouse retraction. It is therefore necessary to elucidate the molecular mechanisms that give rise to the longitudinal friction and lateral confinement arising from topological constraints.

In this Letter, we rigorously test the tube model via coarse-grained simulations of a long, free test chain embedded in a fixed-topology cross-linked network—circumventing constraint-release complications from chain-end effects in linear melts. By analyzing the longitudinal and transverse potentials governing tracer chain dynamics, we identify two unreported phenomena: (1) tube dilation driven by local loop flip-flop rearrangements that form transient entanglements with the test chain, and (2) longitudinal subdiffusion induced by tube nonsmoothness. These findings stand in stark contrast to canonical tube model predictions. Topological confinement renormalizes the effective Rouse time upward by several times relative to an unconstrained chain. This increase reflects an additional, multiscale frictional contribution from transient entanglements that is not captured within the standard tube framework; we refer to this contribution as "topological friction."

Starting from a well-equilibrated configuration (simulation details in End Matter), we generate a series of isoconfigurational conformations [25–27] by assigning random initial velocities to simulate for an additional prescribed duration Δt. Neighboring network chains constrain the test chain into a tubelike molecular cloud [Fig. 1(a1)] [26,27]. We define the test chain's primitive path (PP) via time- and sample-averaged monomer positions; monomer distributions yield longitudinal or transverse potentials, $U = -k_B T \ln(p)$, where p is the probability distribution function of the structural deviations. Here, r quantifies the transverse fluctuation of a monomer relative to the PP and is defined as the minimum distance from the instantaneous monomer position to the PP contour. The variable l characterizes the longitudinal displacement of the monomer along the PP, defined as $l = |i - j|$, where i is the monomer's rank on the polymer backbone and j is the rank index on the PP corresponding to the monomer's nearest projection point; see Fig. 1(a1) and Supplemental Material [28] for detailed mathematical definitions. Figure 1(a2) shows an energy-minimized PP representation of the test chain and network.

In Figs. 1(b) and 1(c), we show the time evolution of the longitudinal potential as a function of the monomer rank along the test chain ($\mathrm{ID}_{\mathrm{mon}}$) for two different test chains. The tube model predicts longitudinal potential heterogeneity in unconstrained chains should smooth on τ_e-scale times. However, for all the test chains, significant heterogeneity persists at $t \approx 100\tau_e$; 1/6 of chains (32 across eight samples) retain notable heterogeneity upto $375\tau_e = \tau_R$. These results suggest that the tubes are rugged in the longitudinal direction, are time-dependent on timescales much longer than τ_e, and possess significant sample variation, highlighting the complex spatiotemporal nature of the topological constraints.

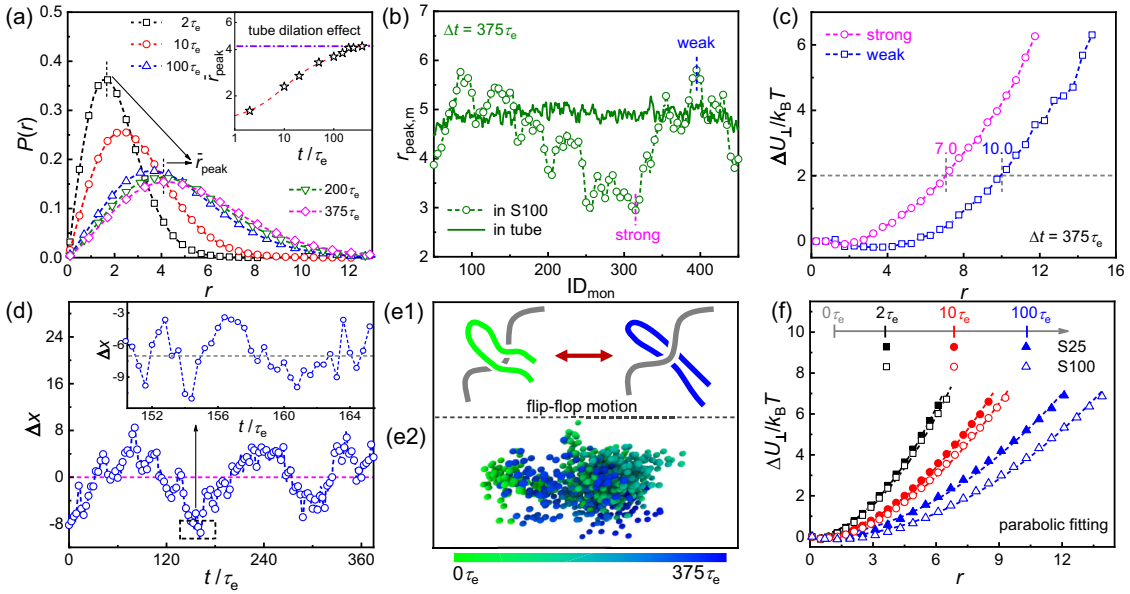

FIG. 2. Transverse potentials. (a) Radial distribution of monomer-to-PP distance, $P(r)$, averaged over all test chains and monomers with $201 \leq \mathrm{ID}_{\mathrm{mon}} \leq 300$ across different timescales. Inset shows the evolution of the most probable radius $\bar{r}_{\mathrm{peak}}$ over time. (b) Variation of the most probable radius $r_{\mathrm{peak,m}}$ with the monomer rank $\mathrm{ID}_{\mathrm{mon}}$ in a test chain at $\Delta t = 375\tau_{\mathrm{e}}$ ($= \tau_{\mathrm{R}}$ for $N = 500$), based on 2000 isoconfigurational conformations. The green solid line ("in tube") represents result for a test chain placed in a straight, smooth tube, where the chain dynamics exhibit no heterogeneity along the monomer rank of the chain. (c) Comparison of transverse constraint potentials $\Delta U_{\perp}$ at strongly versus weakly restricted sites at $\Delta t = \tau_{\mathrm{R}}$, labeled as "strong" and "weak" in (b). (d) Trajectory of the center-of-mass motion of the middle segment of 50 monomers on a test chain; inset in (d) shows a magnified view at short timescales. (e1) "Flip-flop" rearrangement of a loop strand forming transient entanglement with the test chain. (e2) Molecular clouds of the center-of-mass motion of the middle segment. (f) Comparison of transverse potentials for the test chain in networks with different strand lengths across various timescales. Dashed lines are result of parabolic fitting.

Longitudinal potential heterogeneity reflects local structural inhomogeneity, which we link to entanglement tightness via our recently developed method of primitive paths analysis based on combining energy minimization with the Frenet trihedron geometric analysis [29,30]: we use the magnitude of the PP's local curvature κ as a qualitative proxy for the tightness of entanglement. Figure 1(d) compares κ and the longitudinal potential calculated at time $\Delta t = 2\tau_{\mathrm{e}}$, showing clear correlation in both the peak location and the magnitude. The occasional misalignment is due to the continuous evolution of the test chain over the time interval Δt.

The ruggedness of the tube has a profound effect on chain dynamics, giving rise to additional friction due to the topological interactions. We term this additional friction as "topological friction," a concept that was first proposed in Ref. [32] for an ideal chain in a two-dimensional lattice of fixed point obstacles. To demonstrate the effect of the topological friction, we calculate the mean-square displacement of the center of mass $g_3(t)$ of the free chains in networks with different strand lengths ($S = 25$ and 100, referred to as S25 and S100 samples, respectively). The tube model predicts a plateau in $g_3(t)/t^{1/2}$ over timescales $\tau_{\mathrm{e}} < t < \tau_{\mathrm{R}}$. For S100, an approximate plateau is observed. However, there is noticeable downward deviation reflecting a slowing down relative to unhindered Rouse motion. The downward deviation becomes more pronounced for the S25 sample, manifesting as a clear minimum. This suggests that with increasing degree of entanglement, the tube becomes more rugged, resulting in stronger deviation from the unhindered Rouse motion. This effect is further corroborated by changing the bending stiffness of the test chain in the S100 samples. As shown in Fig. 1(f), with increasing chain stiffness, which increases the degree of entanglement, the slowing down behavior becomes more pronounced.

How does structural heterogeneity affect the transverse potential of a test chain? Figure 2(a) shows that for $t < 100\tau_{\mathrm{e}}$, the radial distribution of monomer position relative to the PP chain $P(r) = 2\pi r p(r)$ shifts to larger r over time. This means that the most probable radius, $\bar{r}_{\mathrm{peak}}$ (see inset), increases with time, suggesting a tube dilation effect that contradicts the tube model's picture of a constant tube size for timescales exceeding τ_{e}. This deviation may explain the observed discrepancy between rheological and neutron scattering measurements on the tube size, considering that neutron scattering measures properties on shorter timescales than rheological measurements. Notably, for $t \geq 100\tau_{\mathrm{e}}$, the tube size saturates.

In addition to the temporal variation, Fig. 2(b) demonstrates that $r_{\mathrm{peak,m}}$ varies with the monomer position along the PP, even for times as long as $t = \tau_{\mathrm{R}}$ (see Ref. [28] for details), highlighting the nonuniform nature of the tubelike

constraint. The tube size can alternatively be defined using an energy criterion. For example, setting a potential threshold to be $2k_BT$, Fig. 2(c) shows that there can be an approximate 43% difference in the effective tube size between strongly and weakly confined locations. In a constraining potential that varies with position, a test chain will experience local compression and expansion, resulting in an entropic effect that contributes to the previously discussed subdiffusive motion in the longitudinal direction. The increased topological friction in the longitudinal friction will in turn alter the structure of the surrounding network, thereby affecting the strength of the constraints. Thus, the longitudinal motion and transverse motion of the polymer chain are interdependent up to timescales of order τ_R. Moreover, Fig. 2(c) indicates that, even at the position with the weakest constraint, the transverse potential remains sufficiently large to keep the chain within the confining tube under equilibrium condition, consistent with the picture of the tube model.

To explore the origin of the transverse potential heterogeneity and the tube dilation effect, we examine the center-of-mass motion of the middle segment of 50 monomers on a test chain over τ_R. Figure 2(d) reveals distinct jiggling and hopping movement of the blob on different observation timescales, suggesting a relaxation mechanism that is not contained in the tube model picture and that current primitive paths analysis methods cannot yet capture. An *in situ* analysis of the configuration reveals a local structural rearrangement involving a flip-flop motion of loop strands around the test chain as shown in Fig. 2(e1) (see Ref. [28] for details). Under the topological constraint imposed by the entangling loops, the blob executes local jiggling motion as shown by the color-coded clustering in Fig. 2(e2), while the flip-flop of these entangling loops results in a hoppinglike motion. The relaxation of these local entangling loop strands can take place on timescales much longer than τ_e. This suggests that, on shorter timescales, these entanglements behave similarly to other types of entanglements that effectively restrict the transverse motion of the test chain, but, over longer timescales, the loop strands lose their constraining effects, resulting in increases in the effective tube size across different locations and timescales as reported in Figs. 2(a) and 2(b). Correspondingly, the average transverse potential decreases with increasing timescale as shown in Fig. 2(f), leading to "tube softening." We note that the tube softening observed here differs fundamentally from both melt-based tube dilation [33–35] and the end-looping-induced constraint release [18]. Melt-based tube softening relies on matrix chain reptation, an effect that vanishes for infinitely long chains; the Zhou-Larson mechanism arises from an "end-loop bypass" effect, which also disappears in the infinite chain limit. In contrast, our cross-linked network completely suppresses matrix reptation. Instead, our tube softening arises from the flip-flop motion of local loop strands—a mechanism that persists for all chain lengths and is operative in both networks and monodisperse long-chain melts.

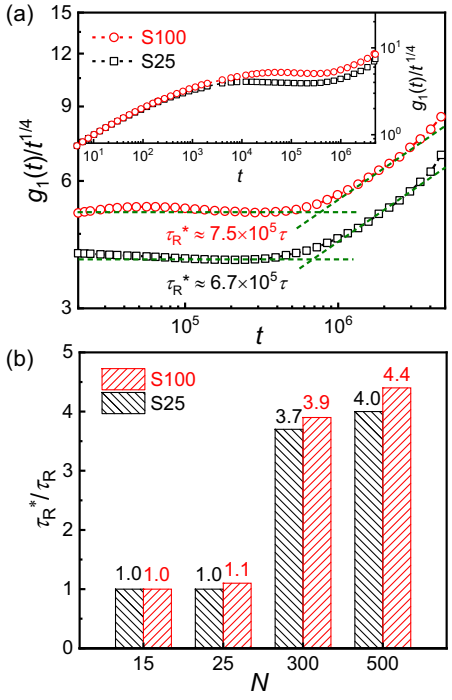

FIG. 3. Mean-square displacement of middle monomers in the test chain $g_1(t)$ and comparison of relaxation times across different systems. (a) Comparison of $g_1(t)$ within S25 and S100 networks. Inset in (a) displays $g_1(t)$ over a longer time span. (b) Ratio of the effective Rouse relaxation times τ_R^* of the test chain in networks with varying strand lengths to the intrinsic Rouse relaxation times τ_R.

Dynamic heterogeneity in longitudinal and transverse potentials strongly modifies the longitudinal relaxation of test chains, which we quantify via the monomer mean-square displacement $g_1(t)$. Extracting the *effective* Rouse relaxation time τ_R^* crossover from $t^{1/4}$ to $t^{1/2}$ scaling [Fig. 3(a)], we find $\tau_R^* \approx 6.7\times10^5\tau$ for S25 and $7.5\times10^5\tau$ for S100. In contrast, *intrinsic* Rouse times τ_R calculated via six established methods (see Ref. [28] for details) yield an average $\tau_R = 1.7\times10^5\tau$. The ratio $\tau_R^*/\tau_R \approx 4.2$ for $N = 500$ (averaged over S25 and S100) and $\tau_R^*/\tau_R \approx 3.8$ for $N = 300$ [Fig. 3(b)] demonstrates that long-timescale dynamic heterogeneity manifests as a Rouse time renormalization, incorporating topological friction from network constraints—directly quantifying topological friction's impact on global dynamics and addressing the uncharacterized local tube statistics identified by Likhtman [36]. Minor τ_R^* differences between S25 and S100 may stem from additional entropic effects. As expected, $\tau_R^* \approx \tau_R$ when test chain length falls below the entanglement strand length N_e [Fig. 3(b)].

To quantify the topological effect, we recall that the Rouse time is related to the friction coefficient as $\tau_R = \zeta_0 N^2 b^2/(3\pi^2 k_B T)$. Although our results demonstrate

heterogeneous dynamics on timescales at or larger than τ_e, for timescales on the order of τ_R or above, the effect of dynamic heterogeneity can be lumped into an effective friction coefficient ζ^* via

$$\tau_R^* = \frac{\zeta^*}{\zeta_0}\tau_R. \quad (1)$$

Writing the effective friction coefficient as a sum of the intrinsic monomer friction coefficient and a contribution due to topological friction,

$$\zeta^* = \zeta_0 + \zeta^{top}, \quad (2)$$

we obtain, from Eqs. (1) and (2), $\zeta^{top} \approx 3.2\zeta_0$ for $N = 500$ and $2.8\zeta_0$ for $N = 300$. The slight difference in ζ^{top} between these two chain lengths is likely due to end effects. For sufficiently long chains, we expect ζ^{top} to be independent of chain length. It should be emphasized that the prefactor treatment of topological friction in Eq. (2) is only valid for long timescales, where the effect of dynamical heterogeneity can be averaged. On short timescales ($<$ loop flip-flop relaxation time), topological friction induces spatiotemporal heterogeneity in the confining potential, leading to a subdiffusive regime with $g_3(t) \sim t^\alpha$ with $\alpha < 1/2$—a qualitative departure from the tube model's predictions [Figs. 1(e) and 1(f)]. These results demonstrate the multiscale character of topological friction.

In conclusion, by probing the dynamics of free polymers in a fixed-topology network—eliminating confounding constraint-release effects—we present a critical re-examination of core tube model assumptions. Our results reveal that chain dynamics remains highly heterogeneous over timescales far exceeding the entanglement time τ_e: the longitudinal potential along the primitive path exhibits persistent ruggedness up to the chain's Rouse time τ_R, while the transverse potential displays nontrivial spatiotemporal structure—including time- and length-scale-dependent softening that cannot be described by a mean-field approximation—that drives tube dilation. We attribute this previously unreported dilation mechanism to flip-flop relaxation of loop-strand entanglements. This dynamic heterogeneity modifies chain dynamics across timescales: for $\tau_e < t < \tau_R$, the test chain's center-of-mass mean-square displacement shows subdiffusive scaling slower than the canonical $t^{1/2}$; at $t \sim \tau_R$, heterogeneity renormalizes the friction coefficient, with our data quantifying the topological friction contribution as roughly 3 times the intrinsic friction. This new topological friction concept unifies short-timescale dynamic heterogeneity and long-timescale quantifiable effects, resolving the classic discrepancy between rheology- and scattering-derived tube sizes.

While focused on fixed-topology networks, our findings stem from two entanglement features omitted in single-chain mean-field theories: discreteness and spatiotemporal heterogeneity. We conjecture analogous behavior arises in sufficiently long polymer melts negligible constraint release and persists—albeit modified—under large, fast deformations ($\dot{\gamma} > 1/\tau_R$). These results highlight the need for entanglement-heterogeneity frameworks to fully describe entangled polymer dynamics in equilibrium and nonequilibrium states.

Acknowledgments—We thank Professor An-Chang Shi (McMaster University) for valuable discussions. This work was supported by the National Key R&D Program of China (2023YFA1008800), the National Natural Science Foundation of China (22341304, 22303100, and 22073092). Z. G. W. acknowledges support from Hong Kong Quantum AI Lab, AIR@InnoHK of Hong Kong Government.

Data availability—There are no publicly available research data or software supporting this manuscript. Requests for further information or data should be sent to the authors.

[1] M. Doi and S. F. Edwards, *The Theory of Polymer Dynamics* (Oxford University Press, New York, 1988).
[2] H. Watanabe, Viscoelasticity and dynamics of entangled polymers, Prog. Polym. Sci. **24**, 1253 (1999).
[3] T. McLeish, Tube theory of entangled polymer dynamics, Adv. Phys. **51**, 1379 (2002).
[4] R. Everaers, S. K. Sukumaran, G. S. Grest, C. Svaneborg, A. Sivasubramanian, and K. Kremer, Rheology and microscopic topology of entangled polymeric liquids, Science **303**, 823 (2004).
[5] S. F. Edwards, The statistical mechanics of polymerized material, Proc. Phys. Soc. **92**, 9 (1967).
[6] S. F. Edwards, The theory of rubber elasticity, Br. Polym. J. **9**, 140 (1977).
[7] P.-G. de Gennes, Reptation of a polymer chain in the presence of fixed obstacles, J. Chem. Phys. **55**, 572 (1971).
[8] J. Higgins and T. McLeish, Travelling by tube, Nature (London) **365**, 205 (1993).
[9] T. McLeish, Polymers without beginning or end, Science **297**, 2005 (2002).
[10] J. Qin and S. T. Milner, Tube dynamics works for randomly entangled rings, Phys. Rev. Lett. **116**, 068307 (2016).
[11] J. Glaser, D. Chakraborty, K. Kroy, I. Lauter, M. Degawa, N. Kirchgeßner, B. Hoffmann, R. Merkel, and M. Giesen, Tube width fluctuations in F-actin solutions, Phys. Rev. Lett. **105**, 037801 (2010).
[12] B. Wang, J. Guan, S. M. Anthony, S. C. Bae, K. S. Schweizer, and S. Granick, Confining potential when a biopolymer filament reptates, Phys. Rev. Lett. **104**, 118301 (2010).
[13] A. F. Behbahani and F. Schmid, Relaxation dynamics of entangled linear polymer melts via molecular dynamics simulations, Macromolecules **58**, 767 (2025).
[14] G. D. J. Phillies, Review: Mean-square displacements of simulated polymers, Polymers **17**, 1193 (2025).

[15] K. L. Ngai, Do entangled polymer chains reptate?, Macromol. Theory Simul. **33**, 202400024 (2024).
[16] D. M. Sussman and K. S. Schweizer, Microscopic theory of entangled polymer melt dynamics: Flexible chains as primitive-path random walks and supercoarse grained needles, Phys. Rev. Lett. **109**, 168306 (2012).
[17] D. M. Sussman and K. S. Schweizer, Entangled polymer chain melts: Orientation and deformation dependent tube confinement and interchain entanglement elasticity, J. Chem. Phys. **139**, 234904 (2013).
[18] Q. Zhou and R. G. Larson, Direct calculation of the tube potential confining entangled polymers, Macromolecules **39**, 6737 (2006).
[19] K. S. Schweizer and S.-J. Xie, Physics of the stress overshoot and chain stretch dynamics of entangled polymer liquids under continuous startup nonlinear shear, ACS Macro Lett. **7**, 218 (2018).
[20] S.-Q. Wang, Nonlinear rheology of entangled polymers at turning point, Soft Matter **11**, 1454 (2015).
[21] S.-Q. Wang, S. Ravindranath, Y. Wang, and P. Boukany, New theoretical considerations in polymer rheology: Elastic breakdown of chain entanglement network, J. Chem. Phys. **127**, 064903 (2007).
[22] Z. Wang, C. N. Lam, W.-R. Chen, W. Wang, J. Liu, Y. Liu, L. Porcar, C. B. Stanley, Z. Zhao, K. Hong, and Y. Wang, Fingerprinting molecular relaxation in deformed polymers, Phys. Rev. X **7**, 031003 (2017).
[23] W.-S. Xu, J.-M. Y. Carrillo, C. N. Lam, B. G. Sumpter, and Y. Wang, Molecular dynamics investigation of the relaxation mechanism of entangled polymers after a large step deformation, ACS Macro Lett. **7**, 190 (2018).
[24] H.-P. Hsu and K. Kremer, Chain retraction in highly entangled stretched polymer melts, Phys. Rev. Lett. **121**, 167801 (2018).
[25] A. Widmer-Cooper, P. Harrowell, and H. Fynewever, How reproducible are dynamic heterogeneities in a supercooled liquid?, Phys. Rev. Lett. **93**, 135701 (2004).
[26] W. Bisbee, J. Qin, and S. T. Milner, Finding the tube with isoconfigurational averaging, Macromolecules **44**, 8972 (2011).
[27] A. E. Likhtman and M. Ponmurugan, Microscopic definition of polymer entanglements, Macromolecules **47**, 1470 (2014).
[28] See Supplemental Material at http://link.aps.org/supplemental/10.1103/cpp1-j6lc for details on (i) simulations for model and method, (ii) calculation of longitudinal and transverse potentials, (iii) flip-flop motion, (iv) heterogeneity of tubelike constraints, and (v) relaxation time calculated from different methods, which includes Refs. [26,29–31].
[29] Y. Ruan, Y. Lu, L. An, and Z.-G. Wang, Nonlinear rheological behaviors in polymer melts after step shear, Macromolecules **52**, 4103 (2019).
[30] Y. Ruan, Y. Lu, L. An, and Z.-G. Wang, Multiple entanglements between two chains in polymer melts: An analysis of primitive paths based on Frenet trihedron, Macromolecules **57**, 2792 (2024).
[31] K. Kremer and G. S. Grest, Dynamics of entangled linear polymer melts: A molecular-dynamics simulation, J. Chem. Phys. **92**, 5057 (1990).
[32] A. K. Omar, Y. Lu, L. An, and Z.-G. Wang, Topological forces in a model system for reptation dynamics, arXiv:2207.05351.
[33] G. Marrucci, Relaxation by reptation and tube enlargement: A model for polydisperse polymers, J. Polym. Sci. **23**, 159 (1985).
[34] J. Viovy, M. Rubinstein, and R. Colby, Constraint release in polymer melts: Tube reorganization versus tube dilation, Macromolecules **24**, 3587 (1991).
[35] D. Read, M. Shivokhin, and A. Likhtman, Contour length fluctuations and constraint release in entangled polymers: Slip-spring simulations and their implications for binary blend rheology, J. Rheol. **62**, 1017 (2018).
[36] A. E. Likhtman, Viscoelasticity and molecular rheology, Polym. Sci. Compr. Ref. **1**, 133 (2012).
[37] A. P. Thompson, H. M. Aktulga, R. Berger, D. S. Bolintineanu, W. M. Brown, P. S. Crozier, P. J. in 't Veld, A. Kohlmeyer, S. G. Moore, T. D. Nguyen, R. Shan, M. J. Stevens, J. Tranchida, C. Trott, and S. J. Plimpton, LAMMPS—A flexible simulation tool for particle-based materials modeling at the atomic, meso, and continuum scales, Comput. Phys. Commun. **271**, 108171 (2022).
[38] R. S. Hoy, K. Foteinopoulou, and M. Kröger, Topological analysis of polymeric melts: Chain-length effects and fast-converging estimators for entanglement length, Phys. Rev. E **80**, 031803 (2009).
[39] M. Kröger, J. D. Dietz, R. S. Hoy, and C. Luap, The Z1+ package: Shortest multiple disconnected path for the analysis of entanglements in macromolecular systems, Comput. Phys. Commun. **283**, 108567 (2023).
[40] J. D. Dietz, M. Kröger, and R. S. Hoy, Validation and refinement of unified analytic model for flexible and semiflexible polymer melt entanglement, Macromolecules **55**, 3613 (2022).
[41] C. Tzoumanekas and D. N. Theodorou, Topological analysis of linear polymer melts: A statistical approach, Macromolecules **39**, 4592 (2006).

End Matter

Simulation details—We employ molecular dynamics simulation on the LAMMPS platform [37] using the Kremer-Grest model for polymer chains [31]. The system is maintained at a reduced temperature of $k_B T = 1$ with a time step of 0.01 in reduced unit. The system consists of 24 free tracer chains with $N = 500$ in a regular three-dimensional diamondlike cross-linked network, where each cross-link has a functionality of 4. The diamondlike cross-linked network, constructed following Doi and Edwards' original framework for isolating tube-scale dynamics, features a well-defined tube length scale while remaining sufficiently simple to be reducible to the original Edwards model [1]. The strand length between adjacent cross-links is set to

$S = 25$ ($S < N_e$) and $S = 100$ ($S > N_e$). Here, $N_e \approx 38$ is the number of monomers within an entanglement strand for a polymer melt, as determined by recent Z1+ topological analysis [38–40]. It should be noted that while N_e is typically defined for melts, its effective value in a network may depend on the strand length S when the mesh size is sufficiently small [41], further contributing to the complexity of the local confining potential. As noted by Hoy *et al.* [38], this value is half that reported by primitive path analysis results reported by Everaers *et al.* [4], reflecting the different definitions of entanglement strands. The density of the system is set at $\rho = 0.85$, with box dimension $12R_{g0} \times 4R_{g0} \times 4R_{g0}$, ensuring an average distance of approximately $2R_{g0}$ between test chains to minimize chain-chain interactions, where $R_{g0} = 12$ is the equilibrium size of a linear chain of $N = 500$ in a polymer melt. The system is allowed to fully equilibrate before data collection. Our simulations are conducted using eight parallel samples. Further details on the model construction and simulation protocol can be found in Supplemental Material [28].